Novel sst_2-Selective Somatostatin Agonists. Three-Dimensional Consensus Structure by NMR

Christy Rani R. Grace,[†] Judit Erchegyi,[‡] Steven C. Koerber,[‡] Jean Claude Reubi,[§] Jean Rivier,*[,‡] and Roland Riek[†]

Structural Biology Laboratory, The Clayton Foundation Laboratories for Peptide Biology, The Salk Institute for Biological Studies, 10010 N. Torrey Pines Road, La Jolla, California 92037, and Division of Cell Biology and Experimental Cancer Research, Institute of Pathology, University of Berne, Berne, Switzerland

Received March 28, 2006

The 3D NMR structures of six octapeptide agonist analogues of somatostatin (SRIF) in the free form are described. These analogues, with the basic sequence H-DPhe/Phe^2-c[Cys^3-Xxx^7-DTrp^8-Lys^9-Thr^{10}-Cys^{14}]-Thr-NH_2 (the numbering refers to the position in native SRIF), with Xxx^7 being Ala/Aph, exhibit potent and highly selective binding to human SRIF type 2 (sst_2) receptors. The backbone of these sst_2-selective analogues have the usual type-II′ β-turn reported in the literature for $sst_{2/3/5}$-subtype-selective analogues. Correlating the biological results and NMR studies led to the identification of the side chains of DPhe^2, DTrp^8, and Lys^9 as the necessary components of the sst_2 pharmacophore. This is the first study to show that the aromatic ring at position 7 (Phe^7) is not critical for sst_2 binding and that it plays an important role in sst_3 and sst_5 binding. This pharmacophore is, therefore, different from that proposed by others for $sst_{2/3/5}$ analogues.

Introduction

Somatostatin (SRIF[a], H-Ala^1-Gly^2-c[Cys^3-Lys^4-Asn^5-Phe^6-Phe^7-Trp^8-Lys^9-Thr^{10}-Phe^{11}-Thr^{12}-Ser^{13}-Cys^{14}]-OH), a cyclic tetradecapeptide isolated from the hypothalamus as a growth hormone inhibitor, is now known to be a multifunctional peptide located in most of the brain regions and in peripheral organs.[1,2] Cells containing SRIF are typically neurons or endocrine-like cells, which are found in high density throughout the central and peripheral nervous systems, in the endocrine pancreas, in the gut, and in small numbers in the thyroid, adrenals, submandibular glands, kidneys, prostrate, and placenta.[1,2] The activities of SRIF are mediated through a family of five different high affinity membrane receptors, sst_1-sst_5 (sst_s). Because of its broad spectrum of physiological activities and its short duration of action due to rapid proteolytic degradation in vivo,[3] SRIF continues to be a target for the development of subtype-specific analogues.[4−7 and refs therein]

Indeed, over the last three decades, hundreds of SRIF analogues have been reported and tested in different biological systems including affinity and selectivity toward the five receptor-subtypes.[8−10] Correspondingly, early structure−activity relationship (SAR) studies ruled out the specific involvement of the side chains of all residues but Phe^7-DTrp^8-Lys^9 for biological recognition.[11−13,63] (Note: the numbering of residues follows that of native SRIF.) Extensive structural studies including NMR and X-ray diffraction[14] were carried out to elucidate the pharmacophore and the consensus structural motif of analogues binding predominantly to $sst_{2/5}$ (and sst_3) receptors.

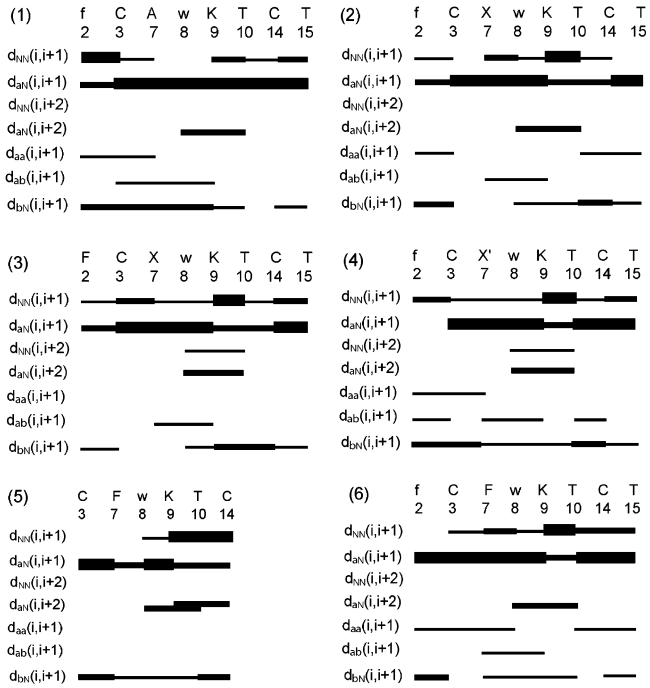

Figure 1. Survey of characteristic NOEs used in CYANA for the structure calculation for analogues **1**−**6**. The thin, medium, and thick bars represent weak (4.5−6 Å), medium (3−4.5 Å), and strong (<3 Å) NOEs observed in the NOESY spectrum. The medium-range connectivities $d_{NN}(i,i+2)$, $d_{\alpha N}(i,i+2)$, and $d_{\beta N}(i,i+2)$ are shown by lines starting and ending at the positions of the residues related by the NOE. The residues designated with X and X′ correspond to amino acids Aph($CONH_2$) and Aph($CONHOCH_3$), respectively.

On the basis of these 3D structures of the free peptides, a pharmacophore model was proposed for SRIF analogues binding to $sst_{2/5}$ (and sst_3).[15−18] In this model, the side chains and the relative spatial arrangement of DPhe^2, Phe^7, DTrp^8, and Lys^9 constitute the most essential elements necessary for binding (Figure 3C). The side chain of DTrp^8 is in close proximity to the side chain of Lys^9 (∼5 Å), whereas the side chain of Phe^7 is about 7−9 Å away from the side chain of DTrp^8 and 9−11 Å from the side chain of Lys^9. The aromatic side chain at position 2, outside the disulfide bond, was not conserved in its

* Corresponding author. Tel: (858) 453-4100. Fax: (858) 552-1546. E-mail: jrivier@salk.edu.

[†] Structural Biology Laboratory, The Salk Institute for Biological Studies.

[‡] The Clayton Foundation Laboratories for Peptide Biology, The Salk Institute for Biological Studies.

[§] University of Berne.

[a] Abbreviations: Amp, 4-aminomethylphenylalanine; Aph, 4-aminophenylalanine; CYANA, combined assignment and dynamics algorithm for NMR applications; DMSO, dimethyl sulfoxide; DQF-COSY, double quantum filtered correlation spectroscopy; IAmp, 4-(*N*-isopropyl)-aminomethyl-phenylalanine; NMR, nuclear magnetic resonance; NOESY, nuclear Overhauser enhancement spectroscopy; 3D, three-dimensional; PROSA, processing algorithms; RMSD, root-mean-square deviation; SAR, structure−activity relationships; SRIF, somatostatin; TOCSY, total correlation spectroscopy.

10.1021/jm060363v CCC: $33.50
Published on Web 07/01/2006

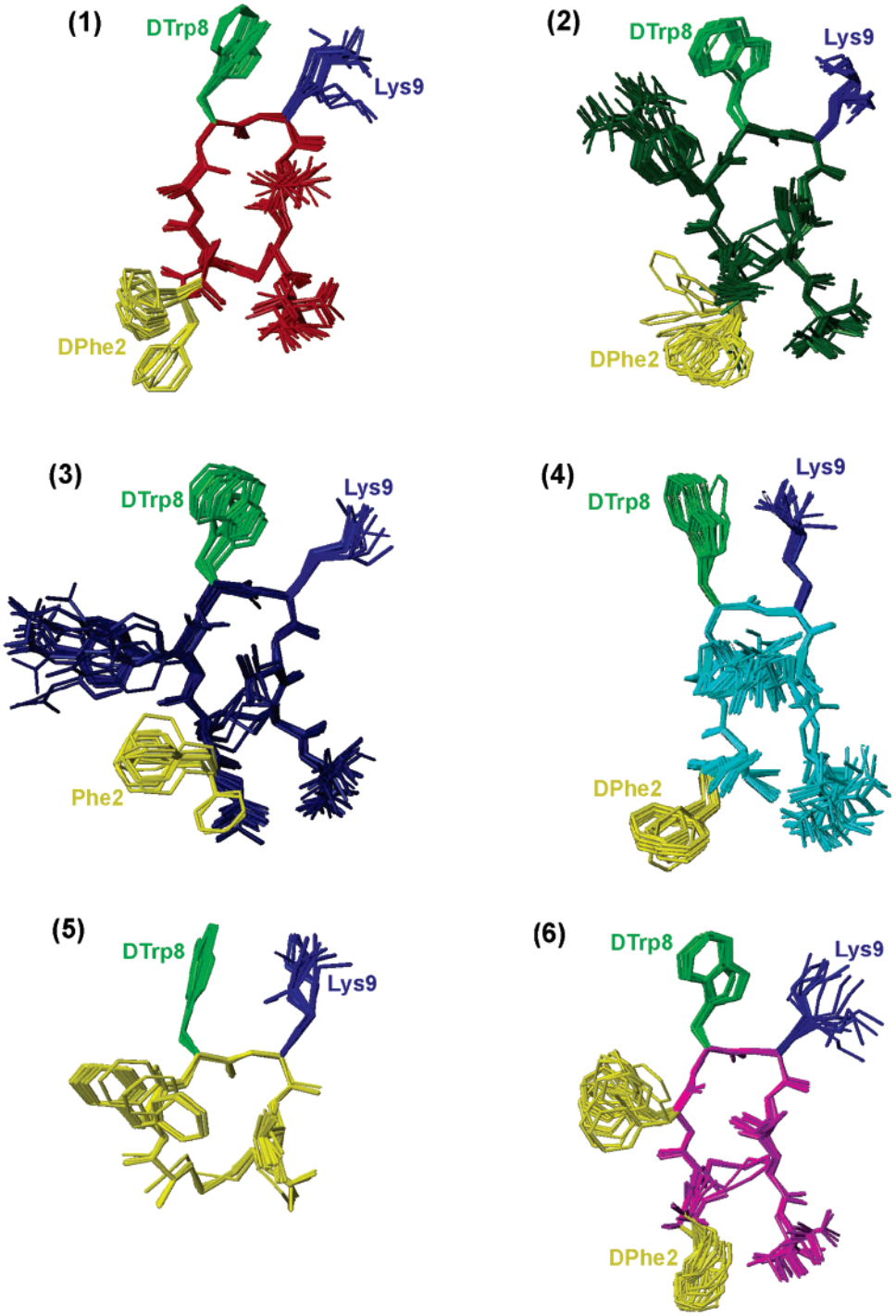

Figure 2. NMR structures of analogues **1**−**6**. For each analogue, 20 energy-minimized conformers with the lowest target function are used to represent the 3D NMR structure. The bundle is obtained by overlapping the C^{α} atoms of residues 2−9. The backbone and side chains are displayed including the disulfide bridge. The following color code is used: red (**1**) H-DPhe-c[Cys-Ala-DTrp-Lys-Thr-Cys]-Thr-NH_2, dark green (**2**) H_2NCO-DPhe-c[Cys-Aph($CONH_2$)-DTrp-Lys-Thr-Cys]-Thr-NH_2, navy blue (**3**) H_2NCO−Phe-c[Cys-Aph($CONH_2$)-DTrp-Lys-Thr-Cys]-Thr-NH_2, cyan (**4**) H_2NCO-DPhe-c[Cys-Aph($CONHOCH_3$)-DTrp-Lys-Thr-Cys]-Thr-NH_2, yellow (**5**) H−c[Cys-Phe-DTrp-Lys-Thr-Cys]-OH, and magenta (**6**) H-DPhe-c[Cys-Phe-DTrp-Lys-Thr-Cys]-Thr-NH_2. The side chains that are involved in sst_2-binding are highlighted; these are DTrp at position 8 in light green, Lys at position 9 in blue, and DPhe or Phe at position 2 in yellow.

position in most of these analogues. The distance between $DPhe^2$ and $DTrp^8$, Lys^9, and Phe^7 was 11−15, 12−15, and 5−11 Å respectively.[19] In this model of the pharmacophore, the rotamer of the side chains of $DTrp^8$ and Phe^7 is in the trans configuration and that of Lys^9 in the gauche configuration.

Recently, we have proposed models of the sst_4 and the sst_1 pharmacophores derived from the NMR consensus structures of several receptor selective analogues.[20,21] These models of the pharmacophores are different from that of the reported $sst_{2/3/5}$ selective pharmacophore in the following manner. The sst_4 pharmacophore has one aromatic side chain, either Phe^6 or Phe^{11} involved in binding in addition to the $DTrp^8$ and Lys^9 pair. The distance between $DTrp^8$ and Lys^9 is 4.5−6.5 Å, between $DTrp^8$ and $Phe^{6/11}$ is 5.5−9.5 Å, and between Lys^9 and $Phe^{6/11}$ is 4.5−6.5 Å. The aromatic side chain of $Phe^{6/11}$ is closer to the side chain of Lys^9 than that of $DTrp^8$ (Figure 3E). However, the sst_1 pharmacophore has two aromatic side chains, at position 6 or 7 and 11, involved in binding in addition to the $DTrp^8$ and $IAmp^9$

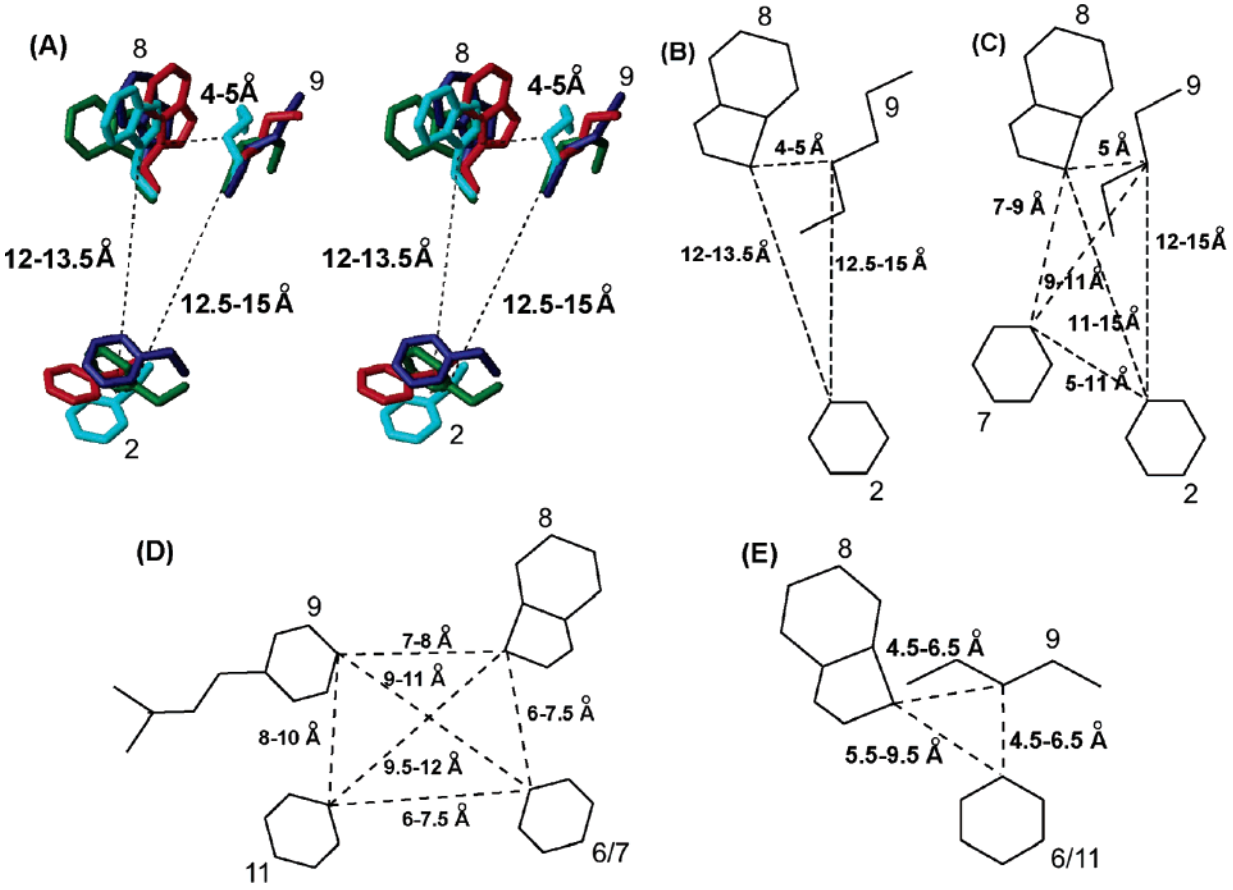

Figure 3. Consensus structural motif of sst$_2$-selective SRIF analogues. (A) Stereo view of the consensus structural motif for the sst$_2$-selective analogues **1** (red), **2** (green), **3** (navy blue), and **4** (cyan). Only the side chains of the residues DPhe^2, DTrp^8, and Lys^9 for **1**, **2**, **3**, and **4** are shown. The distances between the Cγ atoms of DTrp^8, Lys^9, and DPhe^2 are displayed. For each analogue, the conformer with the lowest target function is displayed. (B) Schematic drawing of the pharmacophore for the sst$_2$-selective SRIF analogues. (C) Schematic drawing of the pharmacophore for the sst$_{2/3/5}$-selective SRIF analogues.[16] (D) Schematic drawing of the pharmacophore for the sst$_1$-selective SRIF analogues.[62] (E) Schematic drawing of the pharmacophore for the sst$_4$-selective SRIF analogues.[20] In all of the pharmacophores, the distance between the Cγ atoms of the respective residues is displayed.

pair. The positioning of the two aromatic side chains at the back of the peptide plane has to be noted, which is opposite to that of the sst$_4$ and sst$_{2/3/5}$ pharmacophores. The sst$_1$ receptor selectivity is mainly achieved by the amino acid IAmp, which replaces Lys at position 9. The distance between DTrp^8 and IAmp^9 is 7−8 Å, between DTrp^8 and Phe$^{6/7}$ is 6−7.5 Å, and between IAmp^9 and Phe^{11} is 8−10 Å (Figure 3D).

In a similar manner, we present a model of the sst$_2$ pharmacophore based on the 3D NMR structures of the free peptides. The 3D structures of six analogues in DMSO-d_6 are presented, including the structure of octreotide amide. These analogues have the typical octreotide scaffold with a type-II′ β-turn backbone conformation similar to that of the reported sst$_{2/3/5}$ selective analogues, yet their pharmacophore has one aromatic side chain (Phe^7) less than that of the reported sst$_{2/3/5}$ selective analogues.

Results

Peptide synthesis and characterization are described in Table 1 and Experimental Section.

The proton resonance assignment and the structure determination by NMR for each of the sst$_2$-selective analogues **1**−**6** (Table 1) are presented in Tables 2 and 3.

Assignment of Proton Resonances, Collection of Structural Restraints, and Structure Determination. The nearly complete chemical shift assignment of proton resonances (Table 2) for analogues **1**−**6** (Table 1) has been carried out using two-dimensional (2D) NMR experiments, applying the standard procedure described in the Experimental Section. The *N*-terminal amino protons for analogues **5** and **6** were not observed because of the fast exchange with the solvent. The amide proton of DPhe/Phe^2 for analogues **2** and **3** were observed at high field because of the carbamoylation of the *N*-terminus. Chemical shifts can provide insight into the structure of the peptides, which is particularly true for SRIF analogues. The ring current of the indole ring leads to a distinct shift of the C$^\gamma$ protons of the sequential Lys side chain to lower frequencies when these groups are closer in space, as in a β-turn. The downfield shift of C$^\gamma$ protons has been observed in all of these sst$_2$-selective analogues, which is similar to the observations found in the nonselective analogues binding to sst$_{2/3/5}$.[17,22−30] This indicates the presence of a β-turn around these residues in these analogues.

A large number of experimental NOEs is observed for all of the six analogues in the NOESY spectrum measured with a mixing time of 100 ms, leading to over 100 to 120 meaningful distance restraints per analogue and, concomitantly, ∼15 restraints per residue, which is a typical number for folded proteins (Table 3). These structural restraints are used as input for the structure calculation with the program CYANA[31] followed by restrained energy minimization using the program DISCOVER.[32] The resulting bundle of 20 conformers per analogue represents the 3D structure of each analogue in solution. For each analogue, the small residual constraint violations in the distances for the 20 refined conformers (Table 3) and the coincidence of the experimental NOEs and short

Table 1. Physicochemical Properties and sst_{1-5} Binding Affinities (IC_{50} values, nM) of Analogues Studied by NMR

		purity (%)		MS[c]		IC_{50} nM[d]				
ID #	compound	HPLC[a]	CZE[b]	M(mono) calc.	MH^+(mono) obs.	sst_1	sst_2	sst_3	sst_4	sst_5
1	H-DPhe-c[Cys-Ala-DTrp-Lys-Thr-Cys]-Thr-NH_2	99	99	955.40	956.38	>1 K (3)	8.6;4.5;3.6	772;~1472;543	>1 K (3)	158;807;226
2	H_2N−CO-DPhe-c[Cys-Aph($CONH_2$)-DTrp-Lys-Thr-Cys]-Thr-NH_2	98	97	1132.45	1133.17	>1 K (3)	6.4;9;6.2	210;725;394	>1 K;905;494	400;77;100
3	H_2N−CO−Phe-c[Cys-Aph($CONH_2$) -DTrp-Lys-Thr-Cys] -Thr-NH_2	98	99	1132.45	1133.44	>1 K (2)	7.5;20	942;1094	957;872	109;260
4	H_2N−CO-DPhe-c[Cys-Aph($CONHOCH_3$) -DTrp-Lys-Thr-Cys] -Thr-NH_2	99	99	1119.46	1120.42	>1 K (2)	3.1;4.4	>1 K;958	>1 K (2)	808;539
5	H−c[Cys-Phe-DTrp-Lys-Thr-Cys]-OH	97	98	78430	785.27	>1 K	378	>1 K	>1 K	>1 K
6	H-DPhe-c[Cys-Phe-DTrp-Lys-Thr-Cys] -Thr-NH_2	95	99	1031.43	1032.00	>1 K	2.7;2.2	80;38	>10 K	2.7;3.9

[a] Percent purity determined by HPLC (Hewlett-Packard Series II 1090 Liquid Chromatograph) using buffer systems A = TEAP (pH 2.5) and B = 60% CH_3CN/40% A with a gradient slope of 1% B/min, at a flow rate of 0.2 mL/min on a Vydac C_{18} column (0.21 × 15 cm, 5-μm particle size, 300 Å pore size). Detection at 214 nm. [b] Capillary zone electrophoresis (CZE) was done using a Beckman P/ACE System 2050 controlled by an IBM Personal System/2 Model 50Z and using a ChromJet integrator. Field strength of 15 kV at 30 °C; mobile phase: 100 mM sodium phosphate (85:15, H_2O:CH_3CN) at pH 2.50, on a Supelco P175 capillary tube (363 μm OD × 75 μm ID × 50 cm length). Detection at 214 nm. [c] Mass spectra (MALDI-MS) were measured on an ABI-Perseptive DE-STR instrument. The instrument employs a nitrogen laser (337 nm) at a repetition rate of 20 Hz. The applied accelerating voltage was 20 kV. Spectra were recorded in delayed extraction mode (300 ns delay). All spectra were recorded in the positive reflector mode and were sums of 100 laser shots. The matrix α-cyano-4-hydroxycinnamic acid was prepared as saturated solutions in 0.3% trifluoroacetic acid and 50% acetonitrile. The observed monoisotopic $(M + H)^+$ values of each peptide corresponded with the calculated $(M + H)^+$ values. [d] The IC_{50} values (nM) derived from competitive radioligand displacement assays reflect the affinities of the analogues for the cloned somatostatin receptors using the nonselective ^{125}I-[Leu^8,DTrp^{22},Tyr^{25}]SRIF-28, as the radioligand.

interatomic distances (data not shown) indicate that the input data represent a self-consistent set and that the restraints are well-satisfied in the calculated conformers (Table 3). The deviations from ideal geometry are minimal, and similar energy values are obtained for all of the 20 conformers for each analogue. The quality of the structures determined is reflected by the small backbone RMSD values relative to the mean coordinates of ~0.5 Å (see Table 3 and Figure 2).

Three-Dimensional Structure of H-DPhe^2- c[Cys^3-Ala^7-DTrp^8-Lys^9-Thr^{10}-Cys^{14}]-Thr-NH_2 (1). Analogue **1** binds to receptor 2 with high affinity (IC_{50} < 10 nM) and has an Ala at position 7. The quality of the structure is reflected by the small RMSD (Table 3), which can also be visually depicted from Figure 2 showing the bundle of 20 conformers representing the 3D structure. From the backbone torsion angles (Table 4), it can be seen that the backbone contains a β-turn of type-II′ around DTrp^8-Lys^9. The β-turn is supported by the strong sequential $d_{\alpha N}(i,i+1)$ NOEs and a medium-range $d_{\alpha N}(i,i+2)$ NOE (Figure 1) between DTrp^8 and Thr^{10} as well as the hydrogen bond between Thr^{10}NH-O′Ala^7 in all the 20 structures. The low-temperature coefficient observed for the amide proton of Thr^{10} (−1.1 ppb/K) confirms the presence of the hydrogen bond.[33] From the torsion angles listed in Table 4, it can be seen that the side chain of DTrp^8 is in the trans rotamer, that of Lys^9 in the gauche$^+$ rotamer, and that of DPhe^2 in the gauche$^-$ rotamer.

Three-Dimensional Structure of H_2N-CO-DPhe^2-c[Cys^3-Aph($CONH_2$)^7-DTrp^8-Lys^9-Thr^{10}-Cys^{14}]-Thr-NH_2 (2). Analogue **2** differs from analogue **1** at position 7 by the Aph($CONH_2$) residue as well as the *N*-terminal carbamoylation (Table 1). The backbone torsion angles (Table 4) indicate a β-turn of the type-II′ conformation around DTrp^8-Lys^9, which is supported by the medium-range $d_{\alpha N}(i,i+2)$ NOE between DTrp^8-Thr^{10} (Figure 1). The turn structure is further stabilized by the observed hydrogen bond between Thr^{10}NH-O′Aph^7 in most of the structures. The presence of the hydrogen bond is further confirmed by the unshifted amide proton resonance of Thr^{10} when the temperature was raised from 298 to 313 K. The long-range medium NOE observed between DPhe^2(NH) and Thr^{10}(HN) as well as the strong αH NOE observed between the cysteins stabilize the structure. The side chain of DPhe^2 is in the gauche$^+$ rotamer, those of Aph^7 and DTrp^8 in the trans rotamer, and that of Lys^9 in the gauche$^-$ rotamer (Table 4).

Three-Dimensional Structure of H_2N-CO-DPhe^2-c[Cys^3-Aph($CONH_2$)^7-DTrp^8-Lys^9-Thr^{10}-Cys^{14}]-Thr-NH_2 (3). Analogue **3** binds selectively with high affinity to the sst_2 receptor and is different from analogue **2** with a Phe at position 2. From the backbone torsion angles (Table 4), it can be seen that the backbone contains a β-turn of type-II′ around DTrp^8-Lys^9. The β-turn is supported by the medium-range $d_{\alpha N}(i,i+2)$ NOE and the weak $d_{NN}(i,i+2)$ NOE (Figure 1) between DTrp^8 and Thr^{10} as well as the hydrogen bond Thr^{10}NH-O′Aph^7 observed in most of the 20 structures. The low-temperature coefficient observed for the amide proton of Thr^{10} (−0.4 ppb/K) confirms the presence of the hydrogen bond.[33] In addition, long-range medium NOEs are observed between the amide protons of Phe^2 and Thr^{10} and the cysteines, which stabilizes the structure. The side chains of Phe^2, Aph^7, and Lys^9 are in the gauche$^+$ rotamer, and the side chain of DTrp^8 is in the trans rotamer (Table 4).

Three-Dimensional Structure of H_2N-CO-DPhe^2-c[Cys^3-Aph($CONHOCH_3$)^7-DTrp^8-Lys^9-Thr^{10}-Cys^{14}]-Thr-NH_2 (4). Analogue **4** binds selectively with nanomolar affinity to the sst_2 receptor. It differs from analogues **2** and **3** by the longer chain of Aph($CONHOCH_3$) at position 7, which completely inhibits the binding to receptors 3 and 5 (Table 1). The backbone torsion angles indicate a β-turn of the type-II′ conformation around DTrp^8-Lys^9 (Table 4), which is supported by the medium-range $d_{\alpha N}(i,i+2)$ NOE and the weak $d_{NN}(i,i+2)$ NOE observed between DTrp^8 and Thr^{10} (Figure 1). The unshifted amide proton resonance of Thr^{10} at 7.63 ppm (from 298 to 313 K) suggests the presence of a hydrogen bond involving this amide proton, which has been observed in all of the 20 structures. The side chain of DPhe^2 is in the gauche$^+$ rotamer, those of Aph^7 and

Table 2. Proton Chemical Shifts of Analogues **1**−**6**[a]

		analogues					
residue	^{1}H	**1**	**2**	**3**	**4**	**5**	**6**
H_2N-CO			5.42	5.66	7.59		
DPhe/Phe^2	NH	7.99	6.33	6.42	8.01		
	αH	4.20	4.55	4.53	4.19		4.15
	βH	3.22,	3.08,	3.00,	3.25,		3.24,
		2.96	2.72	2.80	2.95		2.95
	H2,6	7.38	7.28	7.14	7.38		7.38
	H3,5	7.29	7.23	7.21	7.30		7.29
Cys^3	NH	9.22	8.72	8.59	9.23		9.22
	αH	5.27	5.22	5.16	5.27	4.14	5.28
	βH	2.76,	2.77,	2.81,	2.82,	3.07,	2.81,
		2.82	2.77	2.81	2.82	2.98	2.81
		Ala	Aph($CONH_2$)	Aph($CONH_2$)	Aph($CONHOCH_3$)	Phe	Phe
Aph/Ala^7	NH	8.44	8.49	8.45	8.52	8.36	8.55
	αH	4.47	4.58	4.60	4.65	4.67	4.66
	βCH_3	1.17					
	βH		2.77,	2.81,	2.79,	2.81,	2.84,
			2.77	2.81	2.79	2.81	2.84
	H2,6		6.96	6.99	7.03	7.03	7.08
	H3,5		7.22	7.28	7.44	7.16	7.17
	HT		8.46	8.54	8.84		
	NH_2		5.86	5.92	9.55		
	CH_3				3.62		
DTrp^8	NH	8.92	8.82	8.80	8.81	8.74	8.77
	αH	4.30	4.20	4.19	4.19	4.58	4.19
	βH	3.07,	2.98,	2.98,	2.98,	3.14,	2.96,
		2.99	2.73	2.72	2.73	2.86	2.71
	HD1	7.19	6.93	6.91	6.97	6.99	6.95
	HE1	10.87	10.76	10.77	10.74	10.80	10.81
	HZ2	7.32	7.29	7.30	7.29	7.32	7.32
	HH2	7.06	7.04	7.06	7.04	7.08	7.06
	HZ3	6.99	6.98	7.00	6.99	7.00	6.99
	HE3	7.54	7.42	7.41	7.41	7.47	7.43
Lys^9	NH	8.43	8.36	8.39	8.40	8.50	8.46
	αH	3.99	4.01	4.00	3.97	3.89	3.99
	βH	1.70,	1.72,	1.73,	1.70,	1.69,	1.72,
		1.25	1.27	1.29	1.26	1.37	1.30
	γH	0.72,	0.77,	0.80,	0.76,	0.86,	0.79,
		0.72	0.74	0.76	0.72	0.86	0.79
	δH	1.29,	1.30,	1.32,	1.32,	1.35,	1.35,
		1.29	1.30	1.32	1.32	1.35	1.35
	εH	2.55,	2.56,	2.58,	2.55,	2.60,	2.57,
		2.55	2.56	2.58	2.55	2.60	2.57
	εNH	7.60	7.56	7.62	7.58	7.63	7.62
Thr^{10}	NH	7.68	7.58	7.58	7.63	7.72	7.62
	αH	4.48	4.49	4.51	4.48	4.29	4.50
	βH	3.99	3.97	3.97	4.02	4.18	4.00
	γH	1.05	1.06	1.06	1.08	1.09	1.07
	OH	4.88	4.80	4.83	4.87		
Cys^{14}	NH	8.42	8.46	8.47	8.49	8.08	8.49
	αH	5.15	5.30	5.21	5.15	4.58	5.17
	βH	2.86,	2.85,	2.84,	2.86,	3.14,	2.86,
		2.86	2.85	2.84	2.86	2.86	2.86
Thr^{15}	NH	8.06	8.17	8.13	8.05		8.07
	αH	4.22	4.21	4.23	4.23		4.21
	βH	4.02	4.06	3.93	4.03		4.03
	γH	1.05	1.07	0.99	1.07		1.06
	OH	5.15	5.13	5.07	5.15		
NH_2		7.53,	7.42,	7.43,	7.53,		7.35,
		7.36	7.26	7.35	7.36		7.52

[a] The chemical shifts were measured at 298 K in DMSO in ppm with the internal reference of the DMSO signal at 2.49 ppm.

DTrp^8 in the trans rotamer, and that of Lys^9 in the gauche$^-$ rotamer (Table 4). The other long-range NOEs, which stabilize the structure, are observed between the amide proton of DPhe^2 and the αH proton of Cys^{14} and the αH protons of the cysteins.

Three-Dimensional Structure of H-c[Cys^3-Phe^7-DTrp^8-Lys^9-Thr^{10}-Cys^{14}]-OH (5). Analogue **5** is the shortest analogue, a cyclic hexapeptide containing only the core residues. Analogue **5** was synthesized to identify the role of DPhe^2 in sst_2 binding. Indeed, it did not bind to all of the five receptors (Table 1). From the backbone torsion angles, it can be seen that it has a type-II′ β-turn around DTrp^8 and Lys^9 (Table 4) and that the turn is supported by the presence of the medium-range $d_{\alpha N}$-(i,i+2) NOE observed between DTrp^8 and Thr^{10} (Figure 1) as well as the hydrogen bond observed between Thr^{10}NH-O′Phe^7 in all of the 20 structures. The low-temperature coefficient observed for the amide proton of Thr^{10} (−1.4 ppb/K) confirms

Table 3. Characterization of the NMR Structures of Analogues **1**−**6**[a]

						CFF91 energies (kcal/mol)			residual restraint violations on			
									distances		dihedral angles	
ID#	NOE distance restraints	angle restraints[c]	CYANA target function[b]	backbone RMSD (Å)	overall RMSD (Å)	total energy	Van der Waals	Electro-static	no. ≥0.1 Å	max (Å)	no. ≥ 1.5°	max (deg)
1	131	24	0.005	0.52 ± 0.09	1.03 ± 0.20	178 ± 7	89 ± 4	89 ± 7	0.7 ± 0.1	0.11 ± 0.01	0 ± 0	0 ± 0
2	135	17	0.001	0.44 ± 0.24	0.96 ± 0.30	211 ±10	118 ± 5	93 ± 8	0.2 ± 0.1	0.05 ± 0.01	0 ± 0	0 ± 0
3	130	25	0.003	0.47 ± 0.28	1.07 ± 0.45	204 ± 14	124 ± 11	81 ± 7	0.3 ± 0.1	0.07 ± 0.03	0 ± 0	0 ± 0
4	130	19	0.008	0.73 ± 0.25	1.21 ± 0.31	188 ± 11	116 ± 7	72 ± 6	0.5 ± 0.1	0.10 ± 0.02	0 ± 0	0 ± 0
5	80	14	0.0002	0.08 ± 0.09	0.62 ± 0.19	158 ± 10	86 ± 7	73 ± 13	0.1 ± 0.0	0.03 ± 0.00	0 ± 0	0 ± 0
6	115	24	0.002	0.56 ± 0.14	1.06 ± 0.28	210 ± 14	121 ± 10	89 ± 8	0.4 ± 0.1	0.11 ± 0.02	0 ± 0	0 ± 0

[a] The bundle of 20 conformers with the lowest residual target function was used to represent the NMR structures of each analogue. [b] The target function is zero only if all of the experimental distance and torsion angle constraints are fulfilled and all nonbonded atom pairs satisfy a check for the absence of steric overlap. The target function is proportional to the sum of the square of the difference between the calculated distance and the isolated constraint or van der Waals restraints, and similarly isolated angular restraints are included in the target function. For the exact definition see ref 31.[31] [c] Meaningful NOE distance restraints may include intraresidual and sequential NOEs.[31]

Table 4. Torsion Angles ϕ, ψ, and χ_1 (in deg) of the Bundle of 20 Energy-Minimized Conformers

analogue	angle	D-Phe^2	Cys^3	Ala^7	D-Trp^8	Lys^9	Thr^{10}	Cys^{14}	Thr^{15}
1	ϕ		−33 ± 60	−156 ± 13	72 ± 3	−91 ± 0	−140 ± 4	−156 ± 16	−11 ± 46
	ψ	67 ± 17	87 ± 6	132 ± 3	−146 ± 2	26 ± 1	−149 ± 23	87 ± 8	121 ± 56
	χ_1	108 ± 6	132 ± 3	170 ± 95	−151 ± 3	−128 ± 2	−22 ± 86	176 ± 3	173 ± 54
2				Aph(CONH$_2$)^7					
	ϕ	121 ± 45	−84 ± 35	−178 ± 19	97 ± 14	−103 ± 7	−74 ± 5	87 ± 2	−19 ± 37
	ψ	172 ± 9	117 ± 16	88 ± 9	−113 ± 14	2 ± 6	−137 ± 8	81 ± 8	110 ± 76
	χ_1	115 ± 32	−121 ± 40	−175 ± 14	150 ± 6	−83 ± 7	−43 ± 7	−143 ± 24	−163 ± 58
3		Phe^2		Aph(CONH$_2$)^7					
	ϕ	−149 ± 9	174 ± 38	179 ± 22	95 ± 22	−103 ± 12	−63 ± 5	83 ± 28	−109 ± 59
	ψ	−145 ± 51	110 ± 11	98 ± 20	−108 ± 7	−8 ± 1	−140 ± 5	78 ± 8	48 ± 87
	χ_1	−132 ± 30	−144 ± 24	−126 ± 18	−171 ± 6	−105 ± 1	−39 ± 2	−110 ± 34	−129 ± 76
4		D-Phe^2		Aph(CONHOCH$_3$)^7					
	ϕ	175 ± 6	43 ± 2	−111 ± 8	44 ± 5	−141 ± 4	−143 ± 10	167 ± 71	−83 ± 83
	ψ	41 ± 4	53 ± 5	59 ± 5	−104 ± 3	45 ± 8	165 ± 52	78 ± 14	105 ± 78
	χ_1	98 ± 6	−76 ± 34	−177 ± 5	160 ± 5	−45 ± 8	−52 ± 7	−155 ± 13	118 ± 49
5				Phe^7					
	ϕ			−154 ± 8	156 ± 3	−93 ± 3	−93 ± 3	−54 ± 5	
	ψ		168 ± 2	23 ± 6	−128 ± 3	12 ± 0	2 ± 4		
	χ_1		−28 ± 3	160 ± 38	166 ± 1	−116 ± 0	−62 ± 8	−156 ± 4	
6				Phe^7					
	ϕ		−71 ± 28	−173 ± 11	102 ± 2	−93 ± 3	−104 ± 5	−168 ± 5	−89 ± 64
	ψ	−160 ± 0	−153 ± 66	98 ± 6	−121 ± 0	1 ± 3	45 ± 5	81 ± 3	98 ± 70
	χ_1	32 ± 0	−117 ± 5	−150 ± 29	−168 ± 1	−126 ± 4	140 ± 8	−148 ± 12	175 ± 4

the presence of the hydrogen bond.[33] The side chains of Phe^7 and D-Trp^8 are in the trans rotamer, and the side chain of Lys^9 is in the gauche$^+$ rotamer (Table 4).

Three-Dimensional Structure of H-D-Phe^2-c[Cys^3-Phe^7-D-Trp^8-Lys^9-Thr^{10}-Cys^{14}]-Thr-NH$_2$ (6). Analogue **6**, which is very similar to octreotide (Thr-ol is substituted by Thr-NH$_2$), binds to the sst$_{2/3/5}$ receptors with moderately high affinity (Table 1). The 3D structure of this analogue was obtained to compare the structure of octreotide with the other analogues under identical conditions. Melacini et al. reported that the backbone of Sandostatin (octreotide) could be in a conformational equilibrium between the β-turn and the helical structures in solvents different from DMSO.[19,28] From the torsion angles, we observed a type-II′ β-turn conformation for the backbone, which is supported by the presence of the medium-range $d_{\alpha N}(i,i+2)$ NOE observed between D-Trp^8 and Thr^{10} (Figure 1) as well as the hydrogen bond observed between Thr^{10}NH-O′Phe^7 in all of the 20 structures. The unshifted amide proton resonance of Thr^{10} at 7.58 ppm (from 298 to 313 K) confirms that this amide proton is involved in a hydrogen bond. The side chains of Phe^7 and D-Trp^8 are in the trans rotamer, and the side chain of Lys^9 is in the gauche$^+$ rotamer (Table 4).

Discussion

We have recently proposed models of the sst$_1$ and sst$_4$ pharmacophores on the basis of the 3D NMR structures of several receptor-selective analogues. The sst$_1$ and sst$_4$ receptors have maximum sequence similarity and, hence, were assumed to be part of one close family, different from the family of sst$_{2/3/5}$ receptors. Yet, the proposed sst$_1$ and sst$_4$ pharmacophores are completely distinct from each other. For example, the position and the number of aromatic rings involved in binding are different for the two ligands, suggesting that these hydrophobic residues interact with different regions of the sst$_1$ and sst$_4$ receptors, respectively (Figure 3D and E). However, most of the previously published analogues binding with high affinity to the sst$_2$ receptor were also binding to sst$_5$ receptor, and sometimes to sst$_3$ receptor, with nM affinity. Melacini et al.,

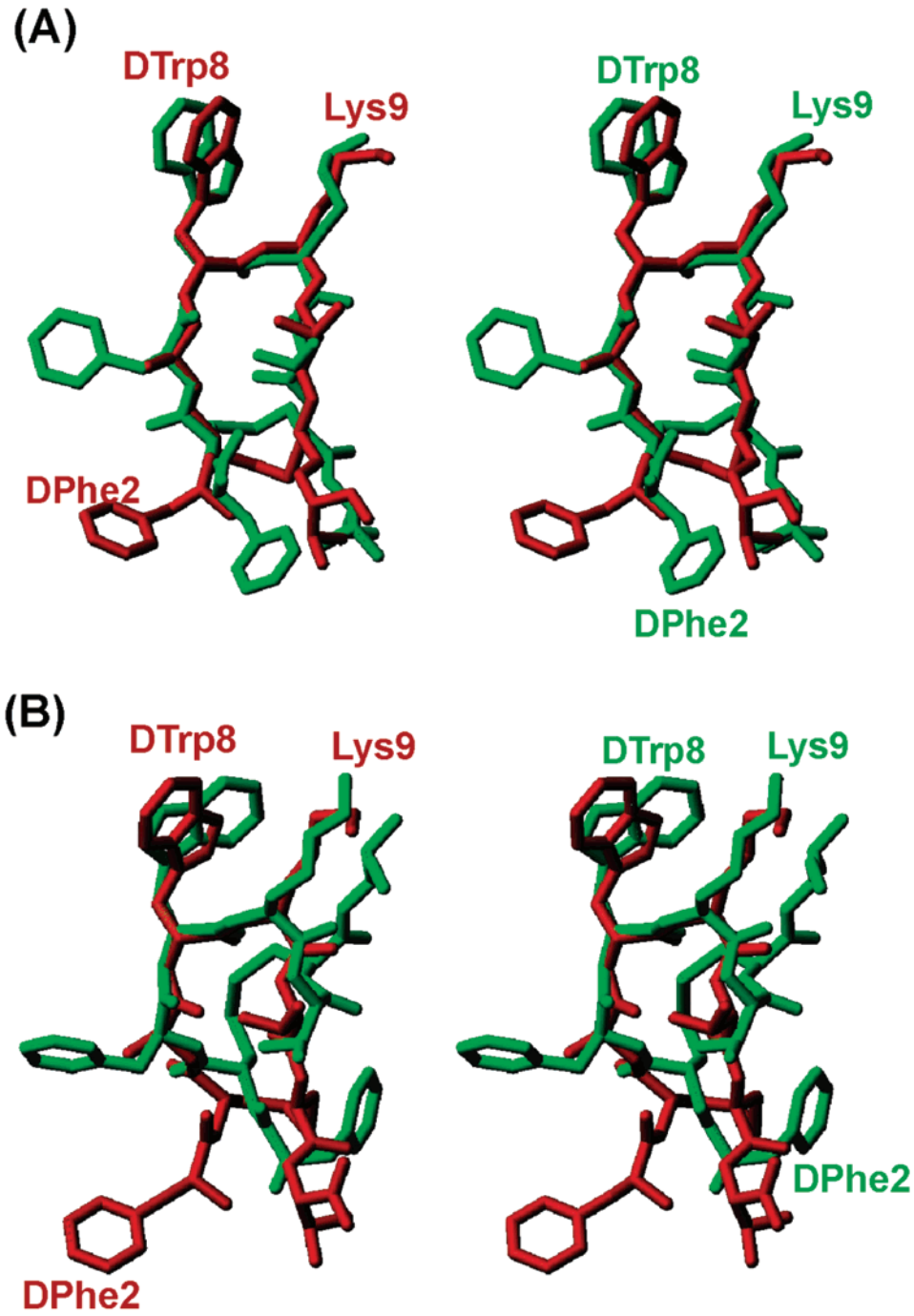

Figure 4. Comparison of the 3D structures of sst$_2$-selective (analogue **1**) and sst$_{2/3/5}$-selective (octreotide and analogue **6**) SRIF analogues. Stereo view of the superposition of the 3D structure of the sst$_2$-selective analogue **1** (red) with the 3D structure of the sst$_{2/3/5}$-selective octreotide (green)[16] (A) in β-turn conformation and (B) in helical conformation. It must be noted that DPhe^2, labeled in both of the analogues, is important for selective binding but differs in its spatial orientation relative to the DTrp^8−Lys^9 pair.

proposed a pharmacophore model for these analogues binding nonselectively to all of the three receptors (Figure 3C).[19] Here, we have identified the crucial residues involved in selective sst$_2$ binding, revealing subtle differences in the pharmacophores between the only sst$_2$-selective analogues and the less selective sst$_{2/3/5}$-selective analogues. In the sst$_{2/3/5}$-selective pharmacophore found in octreotide and homologues, we identified two aromatic side chains (at position 2 and 7) in addition to the DTrp^8 and Lys^9 residues. The removal of the aromatic amino acid at position 2 (analogue **5**) resulted in the loss of binding to all of the three receptors (compare with that in analogue **6**). This clearly confirms that residue 2 is important for binding to sst$_{2/3/5}$ receptors (Table 1). However, the replacement of Phe at position 7 by Ala (analogue **1**) resulted in selective binding (nM) to receptor 2. Hence, it can be concluded that this aromatic ring is not crucial for sst$_2$ binding and that it is crucial for sst$_3$ and sst$_5$ binding as the binding to receptors 3 and 5 decreased (Table 1). The replacement of Phe at position 7 by an amino acid having a longer side chain such as Aph has also decreased the binding to sst$_3$ and sst$_5$ receptors, retaining high binding affinity to sst$_2$ receptors.

Three-Dimensional Structures of the sst$_2$-Selective Analogues and the Pharmacophore Model. Most of the bioactive analogues of SRIF reported so far have a β-turn type of either type II′ or type VI for the backbone conformation.[13,15,17,18,24,34−39] The structures of all of the four sst$_2$-selective analogues

presented also have a β-turn of type-II′ (Figure 2, Table 4). In these analogues, the side chain of DTrp^8 is in the trans conformer, and the side chain of Lys^9 is in either the gauche$^+$ or the gauche$^-$ conformer, bringing the two side chains adjacent to each other in close proximity. The side chain of Phe or DPhe at position 2 is either in the gauche$^+$ or in the gauche$^-$ conformer, far from the DTrp−Lys pair, and their position is conserved in all of the four analogues studied here (Figure 3A). Hence, we propose a pharmacaphore model for sst$_2$-selective analogues involving the three side chains, namely, the indole (DTrp) at position 8, the amino-alkyl (Lys) at position 9, and an aromatic ring at position 2 (Figure 3B). In addition, the right spatial arrangement of the indole ring, the lysine side chain, and the aromatic ring of a phenylalanine is also important for sst$_2$-selective binding. The proposed distance between the Cγ of residue 8 and the Cγ of Phe^2 is 12−13.5 Å, that of Cγ of residue 8 and the Cγ of Lys^9 4−5 Å, and that of the Cγ of Phe^2 and the Cγ of Lys^9 12.5−15 Å. Conservative replacements of these residues do not evidently change the binding affinities and receptor selectivity.

Comparison of the sst$_2$-Selective versus the sst$_{2/3/5}$-Selective Pharmacophore. With the consensus structural motif for the sst$_2$-selective SRIF analogues (Figure 3A and B), a comparison between the sst$_2$ and the pharmacophore for sst$_{2/3/5}$-selective analogues (Figure 3C) is possible. Interestingly, Goodman and co-workers illustrated that in SRIF analogues, which bind selectively to sst$_{2/3/5}$, the side chains of DTrp^8, Lys^9, Phe^7, and Phe^2 constitute the most essential elements necessary for binding.[15,16] In their pharmacophore model, DTrp^8 and Lys^9 were at a close proximity of ∼5 Å, which is similar to the sst$_2$ pharmacophore. The aromatic ring at position 7, Phe^7, is farther away from DTrp^8 (7−9 Å) and Lys^9 (9−11 Å) and is not present in the sst$_2$ pharmacophore. Hence, Phe^7 is not crucial for sst$_2$ receptor binding. The position of DPhe^2 in the sst$_2$ pharmacophore is highly conserved, whereas it varies in the sst$_{2/3/5}$ pharmacophore. This difference can easily be seen from the superposition of the sst$_2$-selective analogue **1** and the sst$_{2/3/5}$-selective octreotide (Figure 4).[16] They differ mostly in the position of the phenylalanine at position 2. On the basis of our studies reported here and the observation of Melacini et al.,[19] octreotide undergoes a conformational exchange between the β-turn and the helical backbone conformation, it can be proposed that octreotide undergoes a conformational change to fit into both the sst$_2$ and sst$_5$ pharmacophores. It should prefer the β-turn conformation, where the DPhe^2 is close to the sst$_2$ pharmacophore (Figure 4A), and prefer the helical conformation to fit the sst$_5$ pharmacophore (Figure 4B), where DPhe^2 is further away from the sst$_2$ pharmacophore (this hypothesis is further supported by the unpublished results of sst$_5$-selective analogues). This conformational flexibility is, therefore, necessary to explain the simultaneous nonselective binding of the octreotide type of analogues to sst$_{2/3/5}$ receptors.

Comparison of the sst$_2$-Selective versus the sst$_1$- and sst$_4$-Selective Pharmacophores. Because three different pharmacophores are available for the subtype-selective analogues, namely, 1, 2 and 4, the differences among these subtype-selective pharmacophores can be discussed with respect to the sst$_2$ pharmacophore (Figure 3B). The sst$_1$ pharmacophore has two aromatic side chains important for binding, and they are closer to the DTrp−IAmp pair and are present on the backside of the peptide, whereas in the sst$_2$ pharmacophore, one aromatic ring important for binding is far from the DTrp−Lys pair. Also IAmp at position 9 crucial for sst$_1$ selectivity is further away from DTrp^8, compared to that in the other pharmacophores, where Lys at position 9 is closer to DTrp^8. The sst$_4$ pharmacophore is somewhat similar to the sst$_2$ pharmacophore in the number of residues interacting with the receptors, namely DTrp^8, Lys^9, and one aromatic side chain at either position 6 or position 11. But the position of the aromatic side chain is closer to the DTrp−Lys pair in the sst$_4$ pharmacophore, whereas it is farther away in the sst$_2$ pharmacophore. Hence, these subtype-selective pharmacophores explain why the sst$_2$-selective analogues did not bind to other receptors of SRIF, specifically to 1 and 4.

Conclusions

The 3D conformations of four cyclic SRIF octapeptide analogues with a hexapeptide core having high binding affinity and selectivity to the sst$_2$ receptor have been presented. These studies indicate that these analogues have a β-turn of type-II′ for the backbone conformation, which orients the side chains of the essentially important residues, namely, the indole at position 8, the amino alkyl group at position 9, and an aromatic ring outside the cycle, in their respective positions for effective receptor−ligand binding. On the basis of this, we have proposed the SRIF binding motif for the sst$_2$ receptor consisting of these three side chains, namely, DTrp^8, Lys^9, and DPhe^2. This binding motif differs from the binding motif for sst$_2$/sst$_3$/sst$_5$-selective receptors by one less aromatic side chain at position 7 (Figure 3). Furthermore, the proposed model also explains the selective binding of the nonpeptoid analogues of SRIF agonists.[40−43] The pharmacophore models proposed so far enable us to understand the binding of several other SRIF analogues to somatostatin receptors and will play an important role in designing highly selective peptides as well as nonpeptide ligands of SRIF.

Experimental Section

Peptide Synthesis, Purification and Characterization. Starting Materials. 4-Methylbenzhydrylamine resin (MBHA) with the capacity of 0.4 mmol/g and Boc-Cys(Mob)-CM resin with a capacity of 0.3−0.4 mmol/g were used. All Boc-N$^\alpha$-protected amino acids were commercially available (Chem Impex, Wood Dale, IL; Reanal Finechemical Co., Budapest, Hungary), except for Boc-Aph(Fmoc), which was synthesized in our laboratory.[44]

Synthesis and Purification. The peptides were synthesized by SPPS methodology following the Boc strategy and purified as published earlier.[45] The −CO-NH$_2$ (Cbm) ureido group at the 4-amino function of Aph and at the *N*-terminus of the peptides was introduced simultaneously on the resin. The 4-amino function of Aph was freed with 20% piperidine in NMP, and the *N*-terminus Boc was deprotected with 50% TFA in DCM after the completion of the synthesis, and then carbamoylation was carried out with NaOCN (200 mg, 1.3 mmol) in NMP (8 mL) and glacial acetic acid (6 mL) per gram of initial resin. The ureido group −CO-NHOCH$_3$ (Cbm-OMe) at the 4-amino function of Aph (analogue **4**) was also introduced on the resin. The *N*$^\alpha$-Boc protected resin-bound hexapeptide Boc-Aph(Fmoc)-DTrp-Lys[Z(2Cl)]-Thr(Bzl)-Cys(Mob)-Thr(Bzl)-MBHA was treated with 20% piperidine in NMP to free the 4-amino function of Aph, and CH$_3$O-NH-COOC$_6$H$_4$-NO$_2$ (10-fold excess) in the presence of DIPEA in NMP was added to the resin, which was shaken at RT for 4 h as described earlier.[46] After the completion of the synthesis, *N*-terminus Boc was deprotected with 50% TFA in DCM, and carbamoylation was carried out as described above. The completed peptides were cleaved from the resin by HF containing the scavengers anisole (10% v/v) and methyl sulfide (5% v/v) for 60 min at 0 °C. The diethyl ether precipitated crude peptides were cyclized in 75% acetic acid (200 mL) by the addition of iodine (10% solution in methanol) until the appearance of a stable orange color. Forty minutes later, ascorbic acid was added to quench the excess iodine. The crude lyophilized peptides were purified by preparative RP-HPLC.[47]

Characterization. The purity of the final peptides was determined by analytical RP-HPLC and CZE analysis.[48] (See Table 1

footnotes for details.) Each peptide showed a purity of >95% by these methods. The observed monoisotopic $(M + H)^+$ values of each peptide corresponded with the calculated $(M + H)^+$ values.

NMR samples were prepared by dissolving 2 mg of the analogue in 0.5 mL of DMSO-d_6. The ^{1}H NMR spectra were recorded on a Bruker 700 MHz spectrometer operating at a proton frequency of 700 MHz. The chemical shifts were measured using DMSO (δ = 2.49 ppm) as an internal standard. The 1D spectra were also acquired at temperatures between 298 and 318 K and were utilized to measure the temperature coefficients of the amide resonances. All 2D spectra were acquired at 298 K. The resonance assignments of the various proton resonances were carried out using total correlation spectroscopy (TOCSY),[49,50] double-quantum filtered spectroscopy (DQF−COSY),[51] and nuclear Overhauser enhancement spectroscopy (NOESY).[52−54] The TOCSY experiments employed the MLEV-17 spin-locking sequence suggested by Davis and Bax,[49] applied for a mixing time of 50 ms. The NOESY experiments were carried out with a mixing time of 100 ms. The TOCSY and NOESY spectra were acquired using 800 complex data points in the ω_1 dimension and 1024 complex data points in the ω_2 dimension with t_{1max} = 47 ms and a t_{2max} = 120 ms and were subsequently zero-filled to 1024 × 2048 before Fourier transformation. The DQF-COSY spectra were acquired with 1024 × 4096 data points and were zero-filled to 2048 × 4096 before Fourier transformation. The TOCSY, DQF-COSY, and NOESY spectra were acquired with 8, 8, and 16 scans, respectively, with a relaxation delay of 1 s. The signal from the residual water of the solvent was suppressed using presaturation during the relaxation delay and during the mixing time. The TOCSY and NOESY data were multiplied by 75° shifted sine-function in both dimensions. All the spectra were processed using the software PROSA.[55] The spectra were analyzed using the software X-EASY.[56]

Structure Determination. The chemical shift assignment of the major conformer (the population of the minor conformer was <10%) was obtained by the standard procedure using DQF-COSY and TOCSY spectra for the intraresidual assignment, and the NOESY spectrum was used for the sequential assignment.[57] The collection of structural restraints was based on the NOEs and vicinal $^3J_{NH\alpha}$ couplings. The dihedral angle constraints were obtained from the $^3J_{NH\alpha}$ couplings, which were measured from the 1D ^{1}H NMR spectra and from the intraresidual and sequential NOEs along with the macro GRIDSEARCH in the program CYANA.[31] The calibration of NOE intensities versus ^{1}H−^{1}H distance restraints and appropriate pseudo-atom corrections to the nonstereospecifically assigned methylene, methyl, and ring protons were performed using the program CYANA. On average, approximately 100 NOE constraints and 20 angle constraints were utilized while calculating the conformers (Table 3). A total of 100 conformers were initially generated by CYANA, and a bundle containing 20 CYANA conformers with the lowest target function values were utilized for further restrained energy minimization, using the CFF91 force field[58] with the energy criteria fit 0.1 kCal/mol/Å[59] in the program DISCOVER with steepest decent and conjugate gradient algorithms.[60] The resulting energy minimized bundle of 20 conformers was used as a basis for discussing the solution conformation of the different SRIF analogues. The structures were analyzed using the program MOLMOL.[61]

Acknowledgment. This work was supported in part by NIH grants DK-50124 and DK-59953. We thank Drs. D. Hoyer, T. Reisine, and S. Schulz for the gift of sst$_{1-5}$ transfected CHO-K1, CCL39, or HEK293 cells. We thank Dr. W. Fisher and W. Low for mass spectrometric analyses, R. Kaiser, C. Miller, and B. Waser for technical assistance in the synthesis and characterization of some peptides and biological testing. We are indebted to D. Doan for manuscript preparation. J.R. is The Dr. Frederik Paulsen Chair in Neurosciences Professor. We thank the H. and J. Weinberg Foundation, the H. N. and F. C. Berger Foundation, and the Auen Foundation for financial support. R.R. is the Pioneer Fund development Chair.

References

(1) Reichlin, S. Somatostatin. *N. Engl. J. Med.* **1983**, *309*, 1495−1501.
(2) Reichlin, S. Somatostatin (second of two parts). *N. Engl. J. Med.* **1983**, *309*, 1556−1563.
(3) Patel, Y. C.; Wheatley, T. In vivo and in vitro plasma disappearance and metabolism of somatostatin-28 and somatostatin-14 in the rat. *Endocrinology* **1983**, *112*, 220−225.
(4) Rivier, J.; Erchegyi, J.; Hoeger, C.; Miller, C.; Low, W.; Wenger, S.; Waser, B.; Schaer, J.-C.; Reubi, J. C. Novel sst$_4$-selective somatostatin (SRIF) agonists. Part I: Lead identification using a betide scan. *J. Med. Chem.* **2003**, *46*, 5579−5586.
(5) Erchegyi, J.; Penke, B.; Simon, L.; Michaelson, S.; Wenger, S.; Waser, B.; Cescato, R.; Schaer, J.-C.; Reubi, J. C.; Rivier, J. Novel sst$_4$-selective somatostatin (SRIF) agonists. Part II: Analogues with β-methyl-3-(2-naphthyl)-alanine substitutions at position 8. *J. Med. Chem.* **2003**, *46*, 5587−5596.
(6) Erchegyi, J.; Waser, B.; Schaer, J.-C.; Cescato, R.; Brazeau, J. F.; Rivier, J.; Reubi, J. C. Novel sst$_4$-selective somatostatin (SRIF) agonists. Part III: Analogues amenable to radiolabeling. *J. Med. Chem.* **2003**, *46*, 5597−5605.
(7) Lewis, I.; Bauer, W.; Albert, R.; Chandramouli, N.; Pless, J.; Weckbecker, G.; Bruns, C. A novel somatostatin mimic with broad somatotropin release inhibitory factor receptor binding and superior therapeutic potential. *J. Med. Chem.* **2003**, *46*, 2334−2344.
(8) Moller, L. N.; Stidsen, C. E.; Hartmann, B.; Holst, J. J. Somatostatin receptors. *Biochim. Biophys. Acta* **2003**, *1616*, 1−84.
(9) Olias, G.; Viollet, C.; Kusserow, H.; Epelbaum, J.; Meyerhof, W. Regulation and function of somatostatin receptors. *J. Neurochem.* **2004**, *89*, 1057−1091.
(10) Reubi, J. C.; Waser, B.; Schaer, J.-C.; Laissue, J. A. Somatostatin receptor sst1-sst5 expression in normal and neoplastic human tissues using receptor autoradiography with subtype-selective ligands. *Eur. J. Nucl. Med.* **2001**, *28*, 836−846.
(11) Vale, W.; Rivier, C.; Brown, M.; Rivier, J. Pharmacology of TRF, LRF and somatostatin. *Hypothalamic Peptide Hormones and Pituitary Regulation: Advances in Experimental Medicine and Biology*; Plenum Press: New York, 1977; pp 123−156.
(12) Vale, W.; Rivier, J.; Ling, N.; Brown, M. Biologic and immunologic activities and applications of somatostatin analogues. *Metabolism* **1978**, *27*, 1391−1401.
(13) Veber, D. F.; Freidinger, R. M.; Perlow, D. S.; Paleveda, W. J., Jr.; Holly, F. W.; Strachan, R. G.; Nutt, R. F.; Arison, B. H.; Homnick, C.; Randall, W. C.; Glitzer, M. S.; Saperstein, R.; Hirschmann, R. A potent cyclic hexapeptide analogue of somatostatin. *Nature (London)* **1981**, *292*, 55−58.
(14) Pohl, E.; Heine, A.; Sheldrick, G. M.; Dauter, Z.; Wilson, K. S.; Kallen, J.; Huber, W.; Pfaffli, P. J. Structure of octreotide, a somatostatin analogue. *Acta Crystallogr., Sect. D* **1995**, *51*, 48−59.
(15) Huang, Z.; He, Y.; Raynor, K.; Tallent, M.; Reisine, T.; Goodman, M. Side chain chiral methylated somatostatin analogue synthesis and conformational analysis. *J. Am. Chem. Soc.* **1992**, *114*, 9390−9401.
(16) Melacini, G.; Zhu, Q.; Osapay, G.; Goodman, M. A refined model for the somatostatin pharmacophore: Conformational analysis of lanthionine-sandostatin analogues. *J. Med. Chem.* **1997**, *40*, 2252−2258.
(17) Mattern, R.-H.; Tran, T.-A.; Goodman, M. Conformational analyses by ^{1}H NMR and computer simulations of cyclic hexapeptides related to somatostatin containing acidic and basic peptoid residues. *J. Pept. Res.* **1999**, *53*, 146−160.
(18) Mattern, R. H.; Tran, T. A.; Goodman, M. Conformational analyses of cyclic hexapeptide analogues of somatostatin containing arylalkyl peptoid and naphthylalanine residues. *J. Pept. Sci.* **1999**, *5*, 161−175.
(19) Melacini, G.; Zhu, Q.; Goodman, M. Multiconformational NMR analysis of sandostatin (octreotide): Equilibrium between β-sheet and partially helical structures. *Biochemistry* **1997**, *36*, 1233−1241.
(20) Grace, C. R. R.; Erchegyi, J.; Koerber, S. C.; Reubi, J. C.; Rivier, J.; Riek, R. Novel sst$_4$-selective somatostatin (SRIF) agonists. Part IV: Three-dimensional consensus structure by NMR. *J. Med. Chem.* **2003**, *46*, 5606−5618.
(21) Erchegyi, J.; Kirby, D.; Hoeger, C.; Koerber, S. C.; Low, W.; Waser, B.; Eltschinger, V.; Schaer, J.-C.; Cescato, R.; Grace, C. R. R.; Reubi, J. C.; Riek, R.; Rivier, J. E. *Design of somatostatin (SRIF) receptor 1- and 4-selective ligands*. Peptides 2004 − Proceedings of the 3rd International and 28th European Peptide Symposium; Kenes International: Prague, Czech Republic, 2004; pp 180−181.
(22) Wynants, C.; Van Binst, G.; Loosli, H. R. SMS 201−995, a very potent analogue of somatostatin. Assignment of the ^{1}H 500 MHz NMR spectra and conformational analysis in aqueous solution. *Int. J. Pept. Protein Res.* **1985**, *25*, 608−614.
(23) Kessler, H.; Haupt, A.; Schudok, M.; Ziegler, K.; Frimmer, M. Peptide conformations. 49(1): synthesis and structure−activity relationships of side chain modified peptides of cyclo(-D-Pro-Phe-Thr-Lys-Trp-Phe-). *Int. J. Pept. Protein Res.* **1988**, *32*, 183−193.

(24) Mierke, D. F.; Pattaroni, C.; Delaet, N.; Toy, A.; Goodman, M.; Tancredi, T.; Motta, A.; Temussi, P. A.; Moroder, L.; Bovermann, G.; Wünsch, E. Cyclic hexapeptides related to somatostatin. *Int. J. Pept. Protein Res.* **1990**, *36*, 418−432.
(25) He, Y.-B.; Huang, Z.; Raynor, K.; Reisine, T.; Goodman, M. Syntheses and conformations of somatostatin-related cyclic hexapeptides incorporating specific alpha and beta-methylated residues. *J. Am. Chem. Soc.* **1993**, *115*, 8066−8072.
(26) Jaspers, H.; Horváth, A.; Mezö, I.; Kéri, G.; Van Binst, G. Conformational study of a series of somatostatin analogues with antitumor and/or GH inhibitory activity. *Int. J. Pept. Protein Res.* **1994**, *43*, 271−276.
(27) Gilon, C.; Huenges, M.; Mathä, B.; Gellerman, G.; Hornik, V.; Afargan, M.; Amitay, O.; Ziv, O.; Feller, E.; Gamliel, A.; Shohat, D.; Wanger, M.; Arad, O.; Kessler, H. A backbone-cyclic, receptor 5-selective somatostatin analogue: Synthesis, bioactivity, and nuclear magnetic resonance conformational analysis. *J. Med. Chem.* **1998**, *41*, 919−929.
(28) Mattern, R.-H.; Zhang, L.; Rueter, J. K.; Goodman, M. Conformational analyses of sandostatin analogues containing stereochemical changes in positions 6 or 8. *Biopolymers* **2000**, *53*, 506−522.
(29) Cheng, R. P.; Suich, D. J.; Cheng, H.; Roder, H.; DeGrado, W. F. Template-constrained somatostatin analogues: a biphenyl linker induces a type-V′ turn. *J. Am. Chem. Soc.* **2001**, *123*, 12710−12711.
(30) Jiang, S.; Gazal, S.; Gelerman, G.; Ziv, O.; Karpov, O.; Litman, P.; Bracha, M.; Afargan, M.; Gilon, C.; Goodman, M. A bioactive somatostatin analogue without a type II′ beta-turn: synthesis and conformational analysis in solution. *J. Pept. Sci.* **2001**, *7*, 521−528.
(31) Güntert, P.; Mumenthaler, C.; Wüthrich, K. Torsion angle dynamics for NMR structure calculation with the new program DYANA. *J. Mol. Biol.* **1997**, *273*, 283−298.
(32) Hagler, A. T.; Dauber, P.; Osguthorpe, D. J.; Hempel, J. C. Dynamics and conformational energetics of a peptide hormone: vasopressin. *Science* **1985**, *227*, 1309−1315.
(33) Andersen, N. H.; Neidigh, J. W.; Harris, S. M.; Lee, G. M.; Liu, Z.; Tong, H. Extracting information from the temperature gradients of polypeptide NH chemical shifts. 1. The importance of conformational averaging. *J. Am. Chem. Soc.* **1997**, *119*, 8547−8561.
(34) Arison, B. H.; Hirschmann, R.; Veber, D. F. Inferences about the conformation of somatostatin at a biologic receptor based on NMR studies. *Bioorg. Chem.* **1978**, *7*.
(35) Kessler, H.; Griesinger, C.; Lautz, J.; Muller, A.; van Gunsteren, W. F.; Berendsen, H. J. C. Conformational dynamics detected by nuclear magnetic resonance NOE values and J coupling constants. *J. Am. Chem. Soc.* **1988**, *110*, 3393−3396.
(36) Huang, A.; Pröbstl, A.; Spencer, J. R.; Yamazaki, T.; Goodman, M. Cyclic hexapeptide analogues of somatostatin containing bridge modifications. *Int. J. Pept. Protein Res.* **1993**, *42*, 352−365.
(37) Mattern, R.-H.; Tran, T.-A.; Goodman, M. Conformational analyses of somatostatin-related cyclic hexapeptides containing peptoid residues. *J. Med. Chem.* **1998**, *41*, 2686−2692.
(38) Falb, E.; Salitra, Y.; Yechezkel, T.; Bracha, M.; Litman, P.; Olender, R.; Rosenfeld, R.; Senderowitz, H.; Jiang, S.; Goodman, M. A bicyclic and hsst2 selective somatostatin analogue: design, synthesis, conformational analysis and binding. *Bioorg. Med. Chem.* **2001**, *9*, 3255−3264.
(39) Veber, D. F. Design and discovery in the development of peptide analogues. *Peptides: Chemistry and Biology*, Twelfth American Peptide Symposium; Cambridge, MA, June 16−21, 1991; pp 1−14.
(40) Ankersen, M.; Crider, M.; Liu, S.; Ho, B.; Andersen, H. S.; Stidsen, C. Discovery of a novel non-peptide somatostatin agonist with SST4 selectivity. *J. Am. Chem. Soc.* **1998**, *120*, 1368−1373.
(41) Liu, S.; Tang, C.; Ho, B.; Ankersen, M.; Stidsen, C. E.; Crider, A. M. Nonpeptide somatostatin agonists with sst_4 selectivity: Synthesis and structure−activity relationships of thioureas. *J. Med. Chem.* **1998**, *41*, 4693−4705.
(42) Rohrer, S. P.; Birzin, E. T.; Mosley, R. T.; Berk, S. C.; Hutchins, S. M.; Shen, D.-M.; Xiong, Y.; Hayes, E. C.; Parmar, R. M.; Foor, F.; Mitra, S. W.; Degrado, S. J.; Shu, M.; Klopp, J. M.; Cai, S.-J.; Blake, A.; Chan, W. W. S.; Pasternak, A.; Yang, L.; Patchett, A. A.; Smith, R. G.; Chapman, K. T.; Schaeffer, J. M. Rapid identification of subtype-selective agonists of the somatostatin receptor through combinatorial chemistry. *Science* **1998**, *282*, 737−740.
(43) Prasad, V.; Birzin, E. T.; McVaugh, C. T.; Van Rijn, R. D.; Rohrer, S. P.; Chicchi, G.; Underwood, D. J.; Thornton, E. R.; Smith, A. B., III; Hirschmann, R. Effects of heterocyclic aromatic substituents on binding affinities at two distinct sites of somatostatin receptors. Correlation with the electrostatic potential of the substituents. *J. Med. Chem.* **2003**, *46*, 1858−1869.
(44) Theobald, P.; Porter, J.; Rivier, C.; Corrigan, A.; Perrin, M.; Vale, W.; Rivier, J. Novel gonadotropin releasing hormone antagonist: Peptides incorporating modified N^{ω}-cyanoguanidino moieties. *J. Med. Chem.* **1991**, *34*, 2395−2402.
(45) Reubi, J. C.; Schaer, J.-C.; Wenger, S.; Hoeger, C.; Erchegyi, J.; Waser, B.; Rivier, J. SST3-selective potent peptidic somatostatin receptor antagonists. *Proc. Natl. Acad. Sci. U.S.A.* **2000**, *97*, 13973−13978.
(46) Samant, M. P.; Grace, C. R. R.; Hong, D. J.; Croston, G.; Riek, R.; Rivier, C.; Rivier, J. Novel analogues of degarelix incorporating hydroxy-, methoxy- and pegylated- urea moieties at residues 3, 5, 6 and the *N*-terminus. Part III. *J. Med. Chem.* **2006**, in press.
(47) Miller, C.; Rivier, J. Peptide chemistry: Development of high-performance liquid chromatography and capillary zone electrophoresis. *Biopolymers Pept. Sci.* **1996**, *40*, 265−317.
(48) Miller, C.; Rivier, J. Analysis of synthetic peptides by capillary zone electrophoresis in organic/aqueous buffers. *J. Pept. Res.* **1998**, *51*, 444−451.
(49) Davis, D. G.; Bax, A. Assignment of complex ^{1}H NMR spectra via two-dimensional homonuclear Hartmann−Hahn spectroscopy. *J. Am. Chem. Soc.* **1985**, *107*, 2820−2821.
(50) Braunschweiler, L.; Ernst, R. R. Coherence transfer by isotropic mixing: Application to proton correlation spectroscopy. *J. Magn. Reson.* **1983**, *53*, 521−528.
(51) Rance, M.; Sorensen, O. W.; Bodenhausen, B.; Wagner, G.; Ernst, R. R.; Wüthrich, K. Improved spectral resolution in COSY1H NMR spectra of proteins via double quantum filtering. *Biochem. Biophys. Res. Commun.* **1983**, *117*, 479−485.
(52) Kumar, A.; Wagner, G.; Ernst, R. R.; Wüthrich, K. Buildup rates of the nuclear Overhauser effect measured by two-dimensional proton magnetic resonance spectroscopy: Implications for studies of protein conformation. *J. Am. Chem. Soc.* **1981**, *103*, 3654−3658.
(53) Macura, S.; Ernst, R. R. Elucidation of cross-relaxation in liquids by two-dimensional NMR spectroscopy. *Mol. Phys.* **1980**, *41*, 95−117.
(54) Macura, S.; Huang, Y.; Suter, D.; Ernst, R. R. Two-dimensional chemical exchange and cross-relaxation spectroscopy of coupled nuclear spins. *J. Magn. Reson.* **1981**, *43*, 259−281.
(55) Güntert, P.; Dotsch, V.; Wider, G.; Wüthrich, K. Processing of multidimensional NMR data with the new software PROSA. *J. Biomol. NMR* **1992**, *2*, 619−629.
(56) Eccles, C.; Güntert, P.; Billeter, M.; Wüthrich, K. Efficient analysis of protein 2D NMR spectra using the software package EASY. *J. Biomol. NMR* **1991**, *1*, 111−130.
(57) Wüthrich, K. *NMR of Proteins and Nucleic Acids*; J. Wiley & Sons: New York, 1986.
(58) Maple, J. R.; Thacher, T. S.; Dinur, U.; Hagler, A. T. Biosym force field research results in new techniques for the extraction of inter- and intramolecular forces. *Chem. Design Auto. News* **1990**, *5*, 5−10.
(59) Koerber, S. C.; Rizo, J.; Struthers, R. S.; Rivier, J. E. Consensus bioactive conformation of cyclic GnRH antagonists defined by NMR and molecular modeling. *J. Med. Chem.* **2000**, *43*, 819−828.
(60) Hagler, A. T. Theoretical simulation of conformation, energetics and dynamics of peptides. *The Peptides: Analysis, Synthesis, Biology*; Academic Press: Orlando, FL, 1985; pp 213−299.
(61) Koradi, R.; Billeter, M. MOLMOL: a program for display and analysis of macromolecular structures. *PDB Newsletter* **1998**, *84*, 5−7.
(62) Grace, C. R. R.; Durrer, L.; Koerber, S. C.; Erchegyi, J.; Reubi, J. C.; Rivier, J. E.; Riek, R. Somatostatin receptor 1 selective analogues: 4. Three-dimensional consensus structure by NMR. *J. Med. Chem.* **2005**, *48*, 523−533.
(63) The abbreviations for the common amino acids are in accordance with the recommendations of the IUPAC−IUB Joint Commission on Biochemical Nomenclature (*Eur. J. Biochem.* **1984**, *138*, 9−37). The symbols represent the L-isomer except when indicated otherwise.

JM060363V